# Radiation patterns of a multiple slit system and applications to organ buffet modeling

Gonzalo Villegas Curulla, Priscila Dalmoro, Benoît Fabre, Brian F.G. Katz

16ème Congrès Français d'Acoustique
11-15 Avril 2022, Marseille

# Radiation patterns of a multiple slit system and applications to organ buffet modeling

G. Villegas Curulla[a,b], P.M.M. Dal Moro[a], B. Fabre[a], and B.F.G. Katz[a]

[a]Sorbonne Université, Institut d'Alembert UMR 7109, LAM, Paris, France
[b]Sorbonne Université, ISCD, Paris, France

The buffet of a pipe organ encloses a complex field created by thousands of pipes acting simultaneously as scatterers and point sources – one in the mouth and one in the passive end, when pipe is not stopped. The facade of the organ, otherwise called *montre*, couples the outside space in the nave with the aforementioned field inside. The main opportunity for field transmission is through the aperture offered by the separation between each of the pipes in the montre. While closed-form models and numerical simulations exist for the transmission through a single slit, the facade of an organ amounts to tens or hundreds of slits thus posing the questions of how to predict the transmitted field and how to group up its behaviour into smaller clusters. An empirically-based approach is followed to provide a description of the field outside the buffet. Measurements were carried out at the near-field and far-field radiation spaces with an experimental scaled model of a positive organ by changing conditions on the number of rigid walls and the density of scatterers.

# 1 Introduction

Modeling musical instruments has become a way to render accessible certain aspects of instruments that are otherwise bound to vanish from collective imagery. It entails an interest, on the one hand, for academic purposes to achieve a higher comprehension of its sounding mechanisms and, on the other hand, an augmentation of such instruments within the context of virtual reality. Pipe organs have been strongly associated with liturgical services and within the confinement of cult spaces. Needless to say, its lack of transportability to laboratories strengthens that prejudice.

In the frame of wind instruments, one seeks to find information along the following axes : the sound production mechanism, coupling mechanisms, the transfer function of the body of the instrument, and the radiation apertures – if the pressure supply at the beginning of the chain is to be left out. For the sake of simplicity, the following assumptions can be made : there is a predominance of flue ranks of pipes over reed ones and, similarly, with non-stopped over stopped pipes, that is, most of them having two open ends.

Pipe ranks inside the buffet are organised in several standard ways inside the buffet, which vary depending on the organ maker and the country and time of its construction. A first major concern to that variability relates to the subdivisions of the interior volume into smaller clusters, e.g. stops in swell box are bound to be found in an independent enclosure. A second one relates to the extent of cluttering, in other words, the density of pipes per squared meter. A last point to make about the internal pipe distribution is the symmetrical chromatic principle generally followed to locate adjacent semitones within the octaves : they are placed on alternating sides within the organ sections (great organ, pedal, positive, etc.) in order to provide spatial balance. Nevertheless, one can imagine that such inverted triangle-like distributions (taller to shorter pipes) will leave vast empty regions with taller pipes leaning towards the side walls of the buffet.

The scope of this study chiefly addresses contributions on the following aspects : the pressure field inside the buffet, the pipe radiation, the filtering effect of the facade, and the field outside the buffet in front of the facade. The eigenmodes of the rigid empty cavity, lossless and without sources, is a well-known consideration [1], whereupon one adds the organ pipes with distinct heights and diameters. For the reasons above, these constitute a $2N_p$ system of radiating monopoles (with $N_p$ eing the number of pipes), on the one hand, and to a great extent heterogenous media of cylinder-like scattering obstacles, on the other. Radiation impedance at the passive end of such cylinders is also well-known case of the unflanged pipe [2] and research effort has also been put forward towards characterising the pipe's mouth impedance [3, 4]. From this point on, it is desirable to gain a better global understanding of the incident field on the slits between the pipes of the facade and the directivity and filtering transformations that it undergoes by propagating through and outwards into the room. For the current work, this has been approached by comparing data from measurements and simulations.

In Sec. 2 the test case and the setup are outlined. Sec. 3 puts forward analytical descriptions of the expected behaviour and compares those with matching simulations. The analysis is extended to acquisitions using the experimental organ in Sec. 4 to conclude with remarks on similarities between patterns observed and what is envisaged to find in further investigations. This study is to be considered complementarily with the companion publication "La boite expressive de l'orgue : étude acoustique de la densité de tuyaux et d'une facade a ouverture variable" by Dal Moro et al. [5], with further dimensioning details and an explicit coordinate system.

# 2 Test cases and setup

To begin, one considers reducing the problem complexity to two dimensions, notwithstanding that studies exist for the whole space with little loss of generality [6, 7]. To this end, an experimental homologue of an organ buffet was built and a scattering matrix of organ pipes was assimilated to an array of equal cross-section cylinders. The two-monopole model for one pipe was substituted by a cylindrical single-source strategy : a line array of in-phase acoustic sources was placed along the third dimension in the locus of one cylinder, while all other pipes were passive scatterers. It is obvious that the experimental buffet is not a real instrument, but a means of isolating elements under measurement. Details on the simulations are given in Sec. 3.2.

The conditions of interest were the presence and number of bounding walls in the buffet, the presence and density of cylinders in the matrix inside the cavity (also referred as the forest [8]), the single or multiple slit radiating system and

the distance from the lines of acquisition to the interface between the inside and outside of the cavity. The aim was to investigate the strength and projection of low-frequency modal responses of the cavity found in the outer domain, pinpointing characteristics that appear across all conditions or only in response to some of them.

The array of scatterers is composed of 170 PVC hollow cylinders with a diameter of $40\,\mathrm{mm}$ cut to a height of $950\,\mathrm{mm}$, embedded into horizontal top and bottom perforated plates made of plexiglass that support all the scatterers in the matrix in place : there are 11 rows and 16 columns available for density combinations, where odd and even rows appear staggered. The pipes are filled with acoustic foam and they serve also the purpose of supporting the acoustic source by clipping it onto any pipe. The source is a vertical array of 18 Aurasound NSW2-326-8A with dimensions $65\,\mathrm{mm} \times 50\,\mathrm{mm} \times 933\,\mathrm{mm}$. The enclosing cavity around is made of plywood panels of $15\,\mathrm{mm}$ thickness supported by a structure of beams : $35\,\mathrm{mm} \times 35\,\mathrm{mm}$ for the section of the four vertical pilar edges and $20\,\mathrm{mm} \times 20\,\mathrm{mm}$ for the rest. The inside dimensions of the cavity are $1340\,\mathrm{mm} \times 580\,\mathrm{mm} \times 980\,\mathrm{mm}$. Five of the cavity panels are removable, allowing for changes in conditions on the walls and for ease of access to the matrix of pipes inside. A window region was cut in the front panel so that interchangeable plexiglass panels can be attached with different slit conditions to the front end of the system. Finally, a small hole was drilled at the bottom of the rear panel in order to pass the wiring necessary for source driving and acquisitions inside the cavity. A Carver PM-175 amplifier was used for the entirety of the experiments to drive the array source.

# 3 Assessment of analytical descriptors

## 3.1 Expected responses from theoretical transfer functions point of view

We attempt to find source-to-system equivalents that resemble the behaviour of acoustic flows and we encapsulate these into a set of transfer functions. The filtering effects expected in the transmitted near-field outside the cavity can be split into three main contributions :

$$H_{buff}(\omega) = H_{bw}(\omega) \cdot H_{sw}(\omega) \cdot H_{MX}(\omega) \tag{1}$$

with $H_{bw}$ expressing the maxima and cancellations seen at a given observation point $O(\vec{r})$ due to phase interference between the arrival of the direct wave-front and the reflected image-source on the back wall of the cavity, being a distance of $2L_{bw}$ from each other, where $|O| \gg L_{bw}$. The parallel side walls of the cavity give rise to eigenmodes for the standing waves encapsulated in $H_{sw}$. Lastly, $H_{MX}$ expresses the the effect of the forest matrix.

The back-wall response for an observation point in the middle front position takes the form :

$$\begin{aligned} H_{bw} &= \frac{P(k,r)}{P_o} \\ &= \frac{1}{\sqrt{r}} e^{-jk(r-L_{bw})}[1 + e^{jk2L_{bw}}] \\ |H_{bw}| &\approx \frac{1}{\sqrt{(r)}} |1 + e^{-j2kL_{bw}}| e^{-j\omega\tau} \end{aligned} \tag{2}$$

where $P_o$ is the reference pressure amplitude, $k_{(\cdot)}$ is the wavenumber and $L_{bw}$ is the distance from the source to the back-wall, yielding $478\,\mathrm{Hz}$ as the first null (for a source-to-wall distance $L_{bw} = 176\,\mathrm{mm}$). The minima shown by the phasor $e^{-j2kL_{bw}}$ at which phase cancellation occurs are distributed in wave number as follows :

$$k_n = \frac{(2n+1)\pi}{2L_{bw}} \tag{3}$$

The presence of the side walls yields pressure maxima and zero velocity on the end-points of the cavity. Its transfer function can be expressed as the ratio $Z = P/U$ between the acoustic flux exciting the cavity and the pressure response :

$$H_{sw} = \frac{1}{j\rho c_o} \frac{\sum_n cos(k_n x)}{\sum_n sin(k_n x)} \tag{4}$$

with $x \in [0, L_{sw}]$, $k_n = n\pi/L_{sw}$, and $L_{sw} = 1340\,\mathrm{mm}$ being the wall-to-wall distance yields a periodicity in spectra of $128\,\mathrm{Hz}$.

Lastly, a forest matrix under infinite extension assumption can be described in terms of wavenumber perturbation :

$$H_{MX} = F(k_{ISA}, \vec{r}) H_{rsc} \tag{5}$$

where $H_{rsc}$ accounts for the scattering phenomena arising from the regularly-spaced cylinders, covered in Sec. 3.2.2. The wavenumber $k_{ISA}$ has undergone a perturbation due to the presence of the forest, whose most salient events are an attenuation of the propagation velocity and pressure amplitude, ultimately shifting downwards the spectra. Some research literature is found to investigate this modified wavenumber, following the infinite-domain extension assumption, and a first order expression named independent scattering approximation (ISA) [9, 10] :

$$k_{ISA}^2 = k_o^2 - j4n_o F(\theta) \tag{6}$$

where $n_o$ is the density of the scattering system and $F(\theta)$ is a scattering function.

The contributions of back-wall and side-wall are seen in Fig. 1, confronting the expected analytical transfer functions and those found in data from simulations. It is seen how the back-wall and side-walls show $478\,\mathrm{Hz}$ and $128\,\mathrm{Hz}$ respectively. The location of side-wall response shown is placed in the middle of the geometry, causing the response to mostly skip over the even-indexed modal frequencies.

## 3.2 Simulations

Numerical equivalents of the study cases in Sec. 2 are simulated using a hybrid FDTD regular hexagonal mesh,

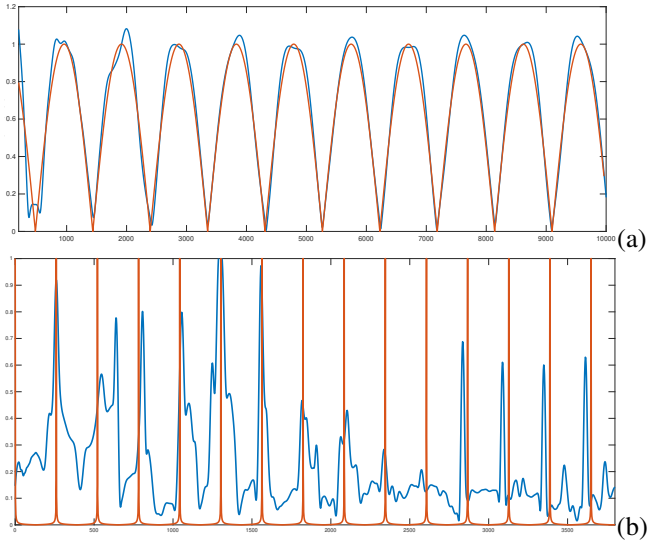


FIGURE 1 – Normalised magnitude of transfer functions of (a) back-wall responses of 3300 time-steps of $P_{tot}/P_{free-field}$ using a Bartlett window and an FFT size of $2^{15}$ samples. (b) Side-walls response over $10^3$ time-steps of $P_{tot}/V_{tot}$ using a Kaiser window ($\beta = 4$), and an FFT size of $2^{17}$ samples. Red and blue solid lines correspond to analytic and simulated responses respectively at an observation point in the vicinity of the interface and slightly off-axis with respect to the source location.

for the domain surrounding the scattering system at hand, with a FVTD mesh circumscribing the rigid bodies, treated as perfectly rigid. The two-dimensional volume cells are adjusted by Voronoi iteration over four buffers around each scatterer to achieve a stable mesh. The outermost buffer couples the FD regular mesh and the FV one. The perimeter of the domain is surrounded by a two-dimensional PML to avoid re-entring propagation from the periodic boundaries.

The excitation conditions injected in the simulation grid is chosen of the form of a scaled Ricker wavelet, this is supported by two reasons : a soft source term is readily differentiated in a wave-equation scheme, with pressure-like dimensions, and a DC contribution is avoided while still adhering to bandwidth and time compactness constraints [11]. CFL is set to 0.95 below the stability condition for the finite volume part proposed in [12].

Data from simulation allows to obtain the field in anechoic conditions : being able to model any realisable condition, one can compute both the reference pressure and the scattered pressure at $O_j(\vec{r})$. This has eased the computation of the arrival time difference between scattered and free propagating waves, which in turn allows comparison with perturbation of wave number model amid the forest media.

The following conditions were simulated :

- 3 walls with no cylinders (back-wall and side-walls)
- 3 walls with facade array of cylinders
- 3 walls with full dense scattering matrix

#### 3.2.1 Rigid empty cavity

Simulations are done to two degrees of detail : once for the sake of the comparability with analytical expressions where geometrical features are reduced to flat planes; secondly with greater geometry detail, for comparability with measured results and analysis of the temporal evolution inside and outside the system. Time domain realisation of the entire domain surrounding the system without any scatterers shows the following (see Fig. 2) :

- First direct arrival wave-front (D) followed by the back-wall's first order reflection (BW) [a]
- First order reflection from the flat panels of side walls (SW) followed by reflections in the bounding inner corners (BW+SWc) [b]
- Progressive structure of standing waves developing across the longest axis of the cavity [c,e,f]
- Scattering from outer bounding edges back onto the back-wall [c]
- Second reflection from BW after initial pulse and shedding of steeper-angle fronts [d]
- Standing wave structure establishes and increases the steeper-angle of the wave fronts reaching outside the cavity [e,f]

#### 3.2.2 Addition of facade and full scattering matrix

It has been shown above how one would expect to find the response of reflections on the main reflective panels (and corners) by means of assuming image-sources relevantly. Next we will see that the addition of the facade and the full dense matrix systems will constitute another direction for image-sources, in the case of the former, situated beyond the facade, and scattering phenomena due to regularly-spaced obstacles in the latter.

Similar issues were explored by D. L. Berry et al. [13] – under (in)finite array assumptions in 1D. They pointed out that some phenomena stronger than the predicted Bragg scattering were observed, referring to them as *quarter-wavelength* frequencies (or *gap* frequencies) because of the similarity between the 3-wall acoustic trap and an organ pipe with open-closed ends – whose first eigenfrequency is ruled by four times its length.

The discussed trap is configured, first, by each two-bounding cylinders where an incident front arrives and, second, by a rigid reflective plane, beyond which the image-sources or image-cylinders are distributed. The pressure terms of the resulting system are :

- Direct source
- Image source
- Cylinder sources
- Image-cylinder sources

In our setups we located source and receivers on opposite sides of the scattering system, thus discarding the image-terms, but the study case of the 1D pipe array

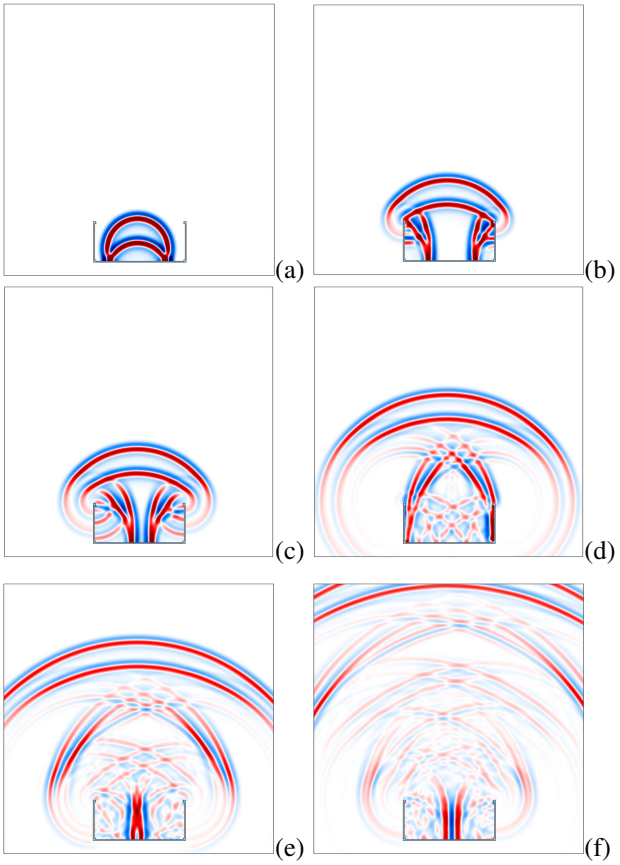


FIGURE 2 – Temporal evolution of the total pressure field around the cavity system without scatterers (pipes). Images correspond to times 1.76 ms, 3.39 ms, 3.94 ms, 6.29 ms, 8.41 ms, and 11.9 ms. Axes are within to the domain dimensions $x \in [-2, 2]$m and $y \in [-0.5, 3.5]$m.

facade remains comparable with the N-cylinders in [13]. In Sec. 4 and 5 numeric detail is provided while compared results from simulations and measurements. One can extend this scattering analysis to the case of the 50% and 100% forest densities without forgetting two aspects : our setup will become an *NxM-cylinder* system and wavenumber modification will start manifestating spectra shifts as mentioned above, but also delays in the arrival times.

The averaged arrival time differences between the free propagation of the source and the equivalent in the scattered pressure field show the influence of the matrix density and its prominence in terms of acquisition proximity to the interface. See Tab. 1, whereby one uses the lossless dispersion relation $c_o = \omega/k_o$ into Eq. 6 to link it with the propagation velocity :

$$c = \alpha \cdot c_o = c_o(1 - \epsilon) = c_o\left(1 - \frac{\tau}{T}\right) \qquad (7)$$

Fig. 3 shows a difference in the integrity of a harmonic structure up to ∼1.5 kHz. Higher-frequency scattering originated by the reasons above is hinted in the regions of 2.5 kHz and 3.1 kHz. Closer examination of the lower frequency structure confirms the aforementioned frequency shift : the clear modal structure with two nulls centered at

TABLEAU 1 – Time difference between the first direct arrival of the freely propagated pulse and that of the scattered field. Arrival times are considered by the −65 dB crossing of the pressure signal normalised by its peak maximum. $T_{scatt}$ is the arrival time of the perturbation to the interface in presence of scattering bodies. Values are averaged for all acquisition points along a line 20 cm in front of the interface.

| | | |
|---|---|---|
| Facade only | $\langle T_{scatt} \rangle$ [ms] | 1.2209 |
| | $\langle \epsilon \rangle \cdot 10^2$ | 0.4032 |
| 100% Forest | $\langle T_{scatt} \rangle$ [ms] | 1.2717 |
| | $\langle \epsilon \rangle \cdot 10^2$ | 3.3568 |

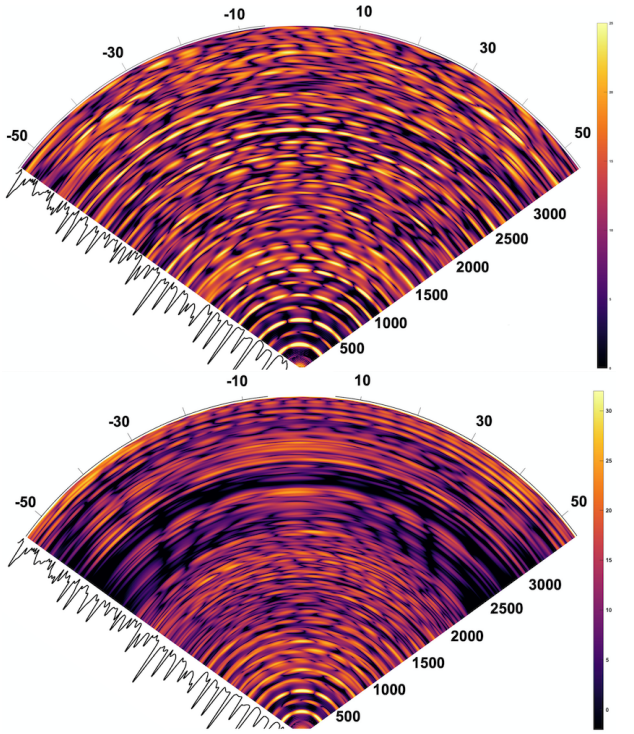


FIGURE 3 – Radiation spectra of simulated pressure, top to bottom : (upper) facade cylinders only and (lower) full dense cylinder matrix ; both in the presence of a 3-wall cavity. The radial axis represents frequency [Hz] and the polar axis expresses the radiation angle for an acquisition distance of 20 cm from the interface and a parallel extension of $[-0.7, 0.7]$m. The scales span 25 and 35 dB respectively.

520 Hz for the *montre* falls to 460 Hz when the full density of scatterers is included, which is in good agreement with experimental results. The dense case shows more clearly the formation of the spatially periodic scattered structure beyond 3 kHz.

# 4 Experiments

The measurements of the transmitted field are made by a finite line of acquisition points in front and parallel to the facade, covering all its width with resolving every 50 mm

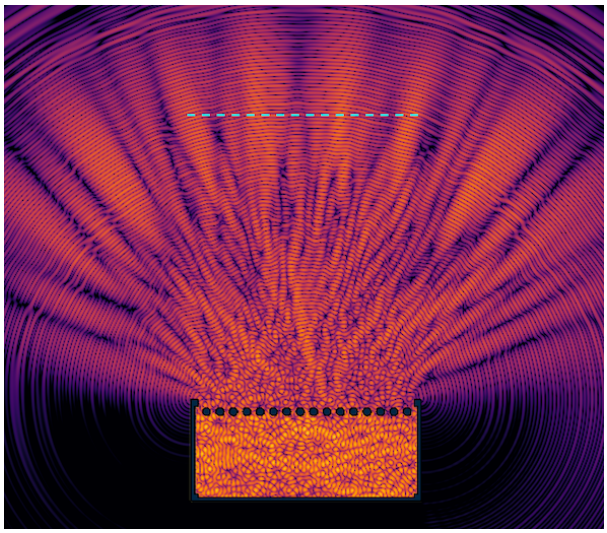

FIGURE 4 – Whole-domain scattered pressure field for 3 walls and facade density conditions. A Chebyshev Type 1 filter pass-band of 7.5 kHz to 8 kHz is applied to the time series at every grid point. Expressed in a dB scale within the range $[-130, -70]$ after normalisation with the incident source pressure.

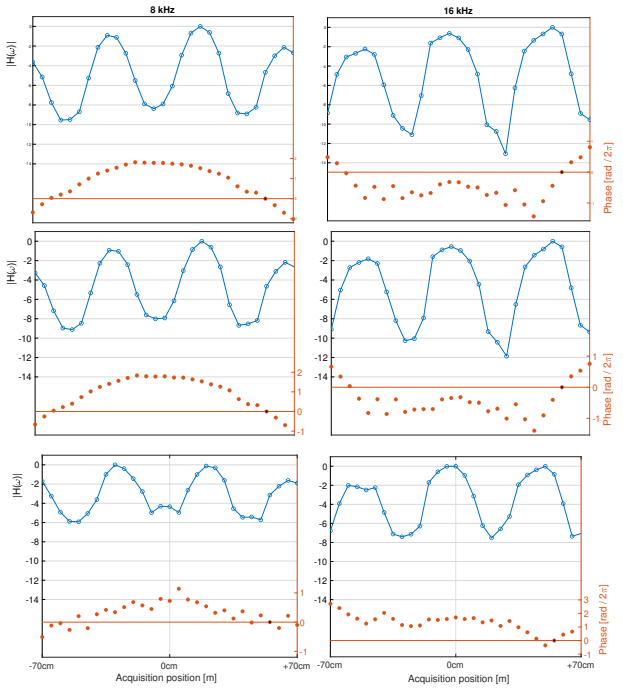


FIGURE 5 – Measured pressure in front of the facade without forest in the interior. Conditions for each row are from top to bottom : (a) anechoic walls, (b) side walls, and (c) all three walls of the cavity. Data is extracted from third octave band analysis. Magnitudes appear in blue with corresponding dB axes on the LHS, superimposed to the phase information (orange) with axis on the RHS.

to a total of 1400 mm. One acquisition line was positioned at 200 mm from the facade, this is 500 mm from source, and another one at 2000 mm from the source. The excitation signal sent to the acoustic source for these experiments was a sinusoidal sweep sampled at 48 kHz ranging from 20 Hz to 20 kHz and lasting 30 s. Study cases measured in an anechoic room respond to the conditions specified in Sec. 2 and Sec. 3.2. Next, most prominent behaviours encountered are described. Bear in mind two setup factors : first, the alignment of the source position does not correspond with the center of the cavity, since it was clipped on the eighth cylinder from the back non-staggered row. Second, the acquisition locations limit the resolvable frequencies, which in the vicinity of the interface can make it unfeasible to capture some phenomena, especially when happening in non-stationary state.

Scattering effects due to regularly-spaced cylinders have a strong prominence in the case of 3 walls with facade cylinders (see Fig. 5) found within the vicinity of the 8 kHz third octave band. The integrity with which the ondulatory behaviour (with a spatial periodicity of $\sim$0.5 m) of the scatterered field in magnitude and phase is mostly disrupted by the presence of the back-wall but not with the presence of side walls. This behaviour appears in the band centerd at 15 849 Hz with the same spatial periodicity but with a sideways shift of the peak position, almost exchanging nulls with peaks. The phase behaviour shows the arrival delay for a cylindrical wave-front to reach a straight acquisition line. These results can be compared with the simulated results in Fig. 4 where the dashed line corresponds to the acquisition line of the measurements at 2 m : the energy in the stationary-state field clearly behaves accordingly to the experimental patterns.

The facade setup and the 50% dense matrix share the same center-to-center distance between cylinders, therefore the same first *quarter-wavelength gap* frequency, estimated around $\sim$1.2 kHz if a length-correction of $0.35d$ is used (where the radiation equivalent for $d$ here expresses the center-to-center distance). The acquisitions at 20 cm from the interface show a $\sim$7 dB peak in the band centered at 3136 Hz. This contribution appears also in the case of the 100% dense, matrix but is most prominently seen at an acquisition distance of 2 m, whereas at 20 cm another $\sim$7 dB peak appears, this time in the band centered around 2512 Hz. By introducing the rest of the scatterers in staggered disposition, the center-to-center distance between cylinders changed from 80 mm to 56.5 mm. This phenomena occur at the same frequency bands independently of wall conditions, where again the addition of the back-wall diminishes the congruence of the side lobes. It leads to believe that the common factor is the presence of the facade.

If we compare the measured and simulated responses (see Fig. 3 and 6), we see that the modal structure in the low frequencies displays the shift behaviour of 530 Hz with only the facade falling to 470 Hz when the full scattering matrix is present. Similarly, the modal structure is more prominent in the case where the field is less perturbed, and the formation of scattering due to evenly-spaced cylinders is seen more clearly while the full staggered grid is present, with the smaller center-to-center spacing, as shown before.

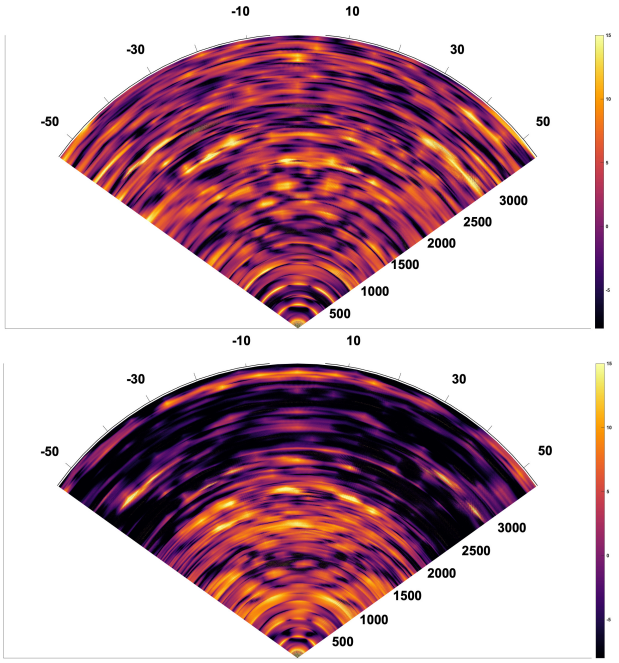


FIGURE 6 – Radiation spectra of measured facade (upper) and full dense cylinder matrix (lower). Data shown (spanning 23 dB) are normalised by the free-field propagation reference pressure of the same setup in absence of any elements of the scattering system.

## 5 Discussion and future work

The current study proposes first-order approximations to the responses of a cavity and a scattering system that behave like an organ buffet. Analytical, simulated, and measured responses show good agreement with respect to cavity responses. We have identified high-frequency patterns caused by regularly-spaced cylinders and showed that the modification of the wavenumber behaved as expected. Further simulations and analysis should be devoted to estimating transfer functions for the far-field directivity, a pseudo-infinite facade pipe array, and an (in)finite scattering matrix forest devoid of cavity. Dispersion analysis was carried out with simulated data but spatio-temporal frequency resolution methods have not yet yield meaningful results in the vicinity of the scatterers of the facade.

The scattering effects analytically estimated, measured and simulated may have been overestimated by the 2D approach under the condition of homogeneously distributed, full-height scatterers. We need to assess how much of the attenuation differences between facade and full dense matrix is due to this overestimation. Further work is envisaged on numerically approximating the radiation from the facade as an array of spaced monopoles of the form :

$$P = \frac{1}{4} k_o \rho_o c_o \sum_{n}^{N_p} q_n e^{-j\phi_n} H_0^-(k_w r_n) \qquad (8)$$

with $q_n$, $\phi_n$, and $r_n$ representing acoustic flow, phase shift and location for each of the $N_p$ monopoles.

Similar measurements were carried out in the empty-buffet and facade conditions in the tribune organ of Notre-Dame de Paris. Preliminary analysis yielded similar high-frequency scattering patterns as those described in this study. They prominently appeared at 5 kHz and 10 kHz center-frequencies. Scaling considerations need to be taken into account in order to make comparisons with measurements in the laboratory : size of the organ cavity, facade center-to-center spacings and pipe diameters.

## Acknowledgements

This work was supported by the Institute of Computing and Data Sciences (ISCD) in Paris.

## Références

[1] L. E. Kinsler, A. R. Frey, A. B. Coppens, and J. V. Sanders, *Fundamentals of Acoustics*. 2000.

[2] A. Chaigne and J. Kergomard, *Acoustics of Musical Instruments*. 2016.

[3] A. Ernoult and B. Fabre, "Window impedance of recorder-like instruments," *Acta Acust United Acust*, 103(1) :106–116, 2017.

[4] P. Rucz, J. Angster, and A. Miklos, "Finite element simulation of radiation impedances with applications for musical instrument design," *Proceedings of ISMA 2019*, no. Sept., 2019.

[5] P. Dal Moro, G. Villegas Curulla, B. Fabre, and C. D'Alessandro, "La boîte expressive de l'orgue : étude acoustique de la densité de tuyaux et d'une façade à ouverture variable," in *Congrès Français d'Acoustique*, 2022.

[6] H. H. Park and H. J. Eom, "Acoustic scattering from a rectangular aperture in a thick hard screen," *J. Acoust. Soc. Am.*, vol. 101, no. 1, pp. 595–598, 1997.

[7] T. Mellow and L. Kärkkäinen, "On the sound fields of infinitely long strips," *J. Acoust. Soc. Am.*, 130(1) :153–167, 2011.

[8] P. Chobeau, *Modeling of sound propagation line matrix method*. PhD thesis, 2014.

[9] A. N. Norris and J.-M. Conoir, "Multiple scattering by cylinders immersed in fluid : High order approximations for the effective wavenumbers," *The J. Acoust. Soc. Am.*, vol. 129, no. 1, pp. 104–113, 2011.

[10] A. Rohfritsch, J.-M. Conoir, R. Marchiano, and T. Valier-Brasier, "Numerical simulation of two-dimensional multiple scattering of sound by a large number of circular cylinders," *J. Acoust. Soc. Am.*, 145(6) :3320–3329, 2020.

[11] J. Sheaffer, M. van Walstijn, and B. Fazenda, "Physical and numerical constraints in source modeling for finite difference simulation of room acoustics," *J. Acoust. Soc. Am.*, vol. 135, no. 1, pp. 251–261, 2014.

[12] S. Bilbao and B. Hamilton, "Passive volumetric time domain simulation for room acoustics applications," *J. Acoust. Soc. Am.*, vol. 145, no. 4, pp. 2613–2624, 2019.

[13] D. L. Berry, S. Taherzadeh, and K. Attenborough, "Acoustic surface wave generation over rigid cylinder arrays on a rigid plane," *J. Acoust. Soc. Am.*, 146(4) :2137–2144, 2019.